



Phase separation and coarsening of NiAl (β') intermetallic in quench-aged Fe–Ni–Al alloys

C. Ferreira-Palma¹ · J. A. Rosas-Barrios² · V. M. López-Hirata² · D. I. Rivas-López² · H. J. Dorantes-Rosales²

Received: 9 September 2019 / Revised: 4 February 2020 / Accepted: 5 February 2020 / Published online: 4 April 2020
© China Iron and Steel Research Institute Group 2020

Abstract

The coarsening behavior of four quench-aged Fe–Ni–Al alloys with different Ni and Al contents is studied. The alloys were solubilized at 1100 °C for 24 h, water-quenched and aged at 850 °C for periods ranging from 1 to 100 h to promote phase separation and coarsening. The two alloys with the highest combined Ni and Al contents (≥ 35 at.%) showed signs of spinodal decomposition, while the alloys with lower Ni and Al contents followed a classical nucleation process. Higher Ni and Al contents promoted an increase in NiAl (β') phase fraction in concordance with phase equilibrium diagrams. The alloy with the highest β' fraction presented a completely interconnected structure. The coarsening of β' particles in the other three alloys followed the predictions of the Lifshitz–Slyozov–Wagner (LSW) theory. The general trend was an increase in the coarsening kinetics with higher Ni and Al contents. The highest hardness was found in the alloys with higher β' fraction albeit these compositions are less resistant to coarsening and have been reported to present a low room-temperature ductility.

Keywords Precipitation · Spinodal decomposition · Coarsening · Aging · Fe–Ni–Al alloy

1 Introduction

The projected requirements for high-temperature materials in steam power generation have increased the interest in several promising candidates [1, 2]. Alloys based on NiAl (β') intermetallic [3, 4] have low density and good high temperature resistance [5], but the lack of room-temperature ductility limits their implementation [6]. Ferritic alloys strengthened with coherent β' precipitates have been extensively studied because of their promising properties [7–9]. The coherent matrix/precipitate relationship present in these alloys is analog to those of Ni-based superalloys, which have proven to provide high temperature resistance [10]. It should be noted that Fe–Ni–Al alloys require further alloying to withstand the projected operational conditions. Cr is usually added to provide improved corrosion resistance [2] and solid-solution strengthening [11]. The simultaneous addition

of Cr and Ti can give rise to hierarchically structured precipitates with very high creep resistance [12–16].

Regarding Fe–Ni–Al system, it has been reported that in quench-aged alloys, the morphology of β' phase is strongly dependent on the alloy composition [17]. Changing the composition gives rise to a variety of possible microstructures including spherical precipitates, cuboidal precipitates, plate-shaped precipitates and, with high Ni and Al contents, an irregular maze-like structure. Regarding this irregular structure, Fe–Ni–Al system presents a miscibility gap strongly influenced by an order–disorder transformation [18]. This can give rise to a spinodal decomposition reaction [19]. This type of reaction has been reported in similar alloys of Fe–Ni–Mn–Al system [20].

Alloys with a moderate amount of Ni and Al present a high coherency between precipitate and matrix, which allows a very low nucleation barrier. After quench-aging treatments, this precipitate/matrix relationship can give rise to finely dispersed nanometric precipitates, which provide excellent strengthening properties on maraging [15, 21, 22] and other precipitation-strengthened steels [23, 24].

An issue to develop further is the analysis of extended aging periods in several quench-aged alloys of Fe–Ni–Al system in order to determine time-dependent behavior such as coarsening kinetics. The determination of the kinetic

✉ C. Ferreira-Palma
carferreira@uv.mx

¹ Faculty of Chemical Sciences, Universidad Veracruzana, Veracruz 94294, Mexico

² ESQIE, Instituto Politécnico Nacional, UPALM, Mexico City 07738, Mexico

constant is important for new alloy developments since the precipitate coarsening resistance has a strong impact on the high-temperature properties of metallic alloys [25]. The objective of this work is to determine the effects of composition and aging time on the microstructural characteristics and coarsening behavior of β' phase in specific compositions of Fe–Ni–Al system.

2 Experimental

For the purposes of this work, four Fe–Ni–Al alloys, with increasing Ni and Al contents, were selected because of their microstructural characteristics [17] and their position in the phase equilibrium diagram [26], covering roughly from the middle of $\alpha + \beta'$ region to the solvus closest to Fe-rich corner (Fig. 1).

Fe–Ni–Al alloys were fabricated from 99% purity elements in an electric arc furnace in Ar atmosphere. The composition of the alloys was analyzed using a scanning electron microscope (JEOL JSM 6300, SEM) equipped with an energy-dispersive spectrometer (Noran System 7, EDS). The nominal and measured compositions along with the proposed nomenclature are detailed in Table 1. The position of

the selected compositions in the phase diagram of Fe–Ni–Al system at 850 °C is presented in Fig. 1 [26]. It is evident that all of the alloys lie in $\alpha + \beta'$ region, where α is the ferritic BCC phase and β' corresponds to NiAl intermetallic with B2-type structure.

The alloys were encapsulated in quartz in an inert atmosphere and homogenized at 1100 °C for 24 h and water-quenched. Subsequently, the specimens were aged at 850 °C for 5, 10, 25, 50 and 100 h.

The specimens were metallographically prepared and polished with 0.05- μm Al_2O_3 . The microstructure was revealed with electrochemically etching using a 10 vol.% HCl–methanol solution with voltages ranging from 0.3 to 1 V during periods ranging from 3 to 15 s.

Microstructural characterization was carried out in a high-resolution scanning electron microscope (JEOL JSM6701F, HR-SEM) at an acceleration voltage of 15 kV and emission current of 20 μA , using the secondary electron detector. The obtained micrographs were processed with the ImageJ image analyzer software which uses a systematic pixel-counting procedure for the determination of areas. This allowed to calculate information such as precipitate area fraction (f_A), average precipitate/plate size, average equivalent radius and size distributions.

Phase identification was carried out by X-ray diffraction (XRD) using a Bruker D8 Focus diffractometer equipped with a collimated Cu $\text{K}\alpha$ source, corrected for fluorescence.

The mechanical behavior during aging was followed using Vickers micro-hardness measurements taken with a Future-Tech hardness tester with a load of 0.98 N and 12 s dwell time.

3 Results and discussion

Figure 2 shows the microstructural evolution of the four alloys during different stages of aging at 850 °C. The bright phase corresponds to β' intermetallic, while the dark phase corresponds to the ferritic α phase. It can be observed that β' fraction tends to increase with higher Ni and Al contents in concordance with the phase equilibrium diagrams and the observations made in a previous work [17].

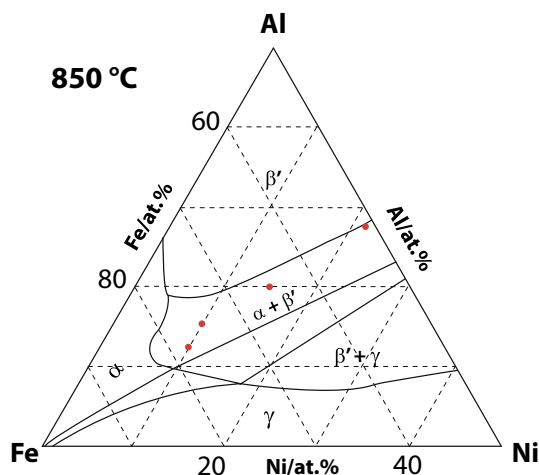


Fig. 1 Analyzed compositions in Fe–Ni–Al phase diagram [26]

Table 1 Composition of selected Fe–Ni–Al alloys (at.%)

Alloy	Nominal			EDS measured		
	Fe	Al	Ni	Fe	Al	Ni
FAN1210	78	12	10	Balance	11.3 ± 0.3	10.0 ± 0.5
FAN1510	75	15	10	Balance	14.6 ± 0.1	9.7 ± 0.3
FAN2015	65	20	15	Balance	19.5 ± 0.4	14.9 ± 0.2
FAN2823	49	28	23	Balance	27.9 ± 0.6	22.9 ± 0.5

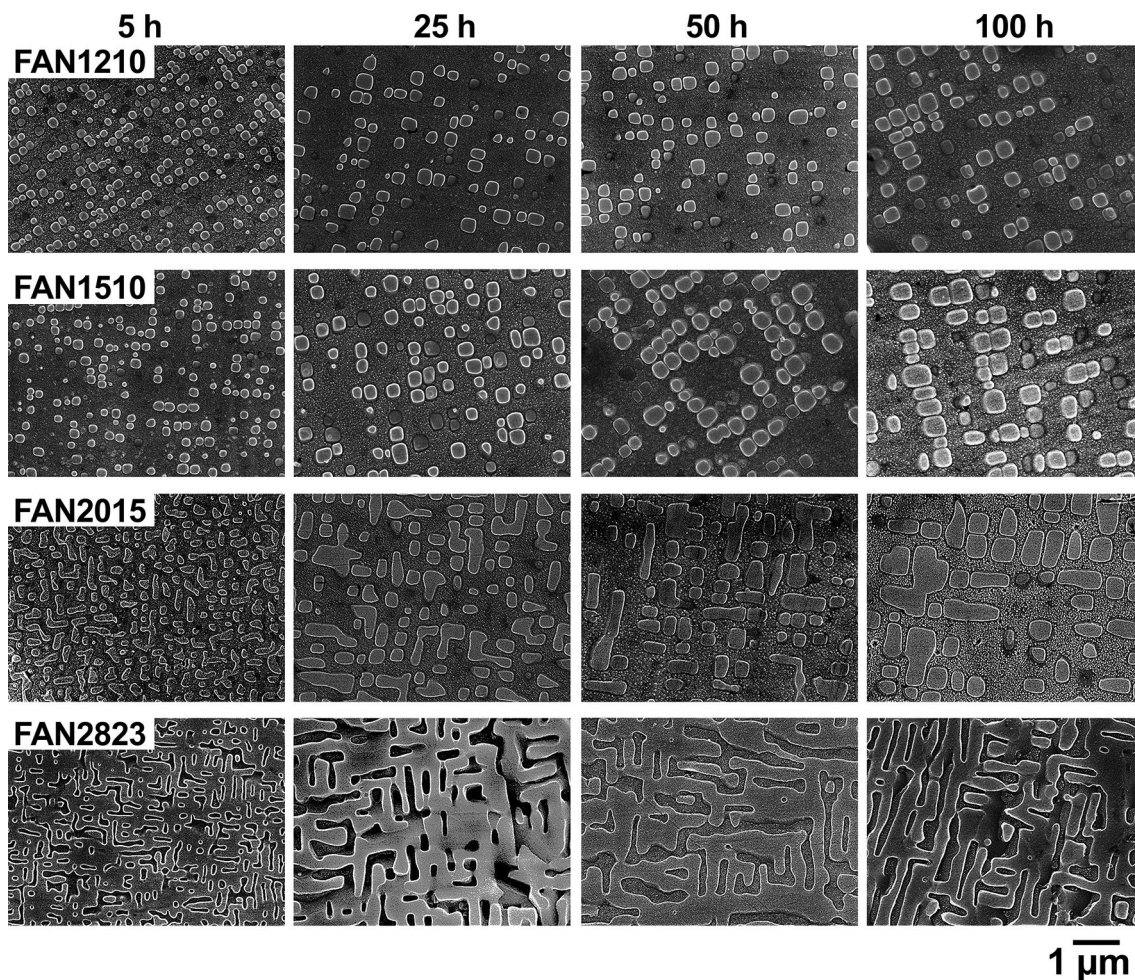


Fig. 2 Microstructural evolution of alloys during aging at 850 °C

It is evident that, for FAN1210, FAN1510 and FAN2015 alloys, the average precipitate size tends to increase during the aging process. This size increase and the morphological changes suggest that coarsening takes place during the aging process. For FAN1210 and FAN1510 alloys, the precipitate morphology consists of spheres after the initial 5 h of aging. In this condition, the precipitates already show signs of alignment in preferential orientations [27]. This kind of alignment has also been observed in Ni-based superalloys [28–31] and is attributed to the interactions between the elastic energies among adjacent precipitates and the effect of the coherent elastic strains between the matrix and precipitates. As the aging process continues, the precipitates of these alloys change to a rounded-cuboid morphology.

β' phase in FAN2015 alloy presents an irregular morphology after 5 h of aging, which evolves to elongated shapes with further aging. The initial irregular morphology is also observed in a shorter aging time (Fig. 3). This microstructure has also been observed in phase field simulations of spinodal decomposition in hypothetical A–B–C systems

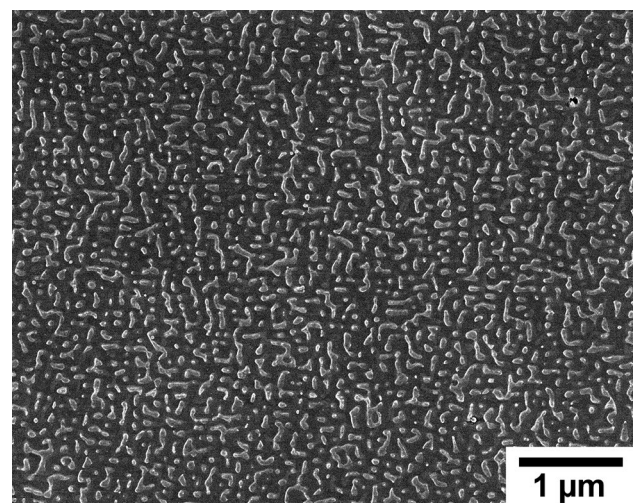


Fig. 3 Microstructure of FAN2015 alloy after 30 min of aging at 850 °C

Table 2 Phase composition after 100 h at 850 °C by EDS

Content/at. %	FAN2823 alloy		FAN1510 alloy	
	α	β'	α	β'
Al	16.4 ± 0.1	25.3 ± 0.6	13.3 ± 0.3	19.6 ± 0.4
Ni	16.0 ± 0.2	22.2 ± 0.5	9.2 ± 0.3	13.5 ± 0.5
Fe	67.6 ± 0.1	52.5 ± 0.4	77.5 ± 0.2	66.9 ± 0.3

with a miscibility gap and anisotropic elastic strain between phases [32].

FAN2823 alloy shows a completely interconnected structure of β' phase surrounding small isolated regions of α phase. Similar alloys which exhibited this behavior [20] have also been reported to follow a spinodal decomposition reaction. Further aging of these alloys promotes the coarsening of α regions.

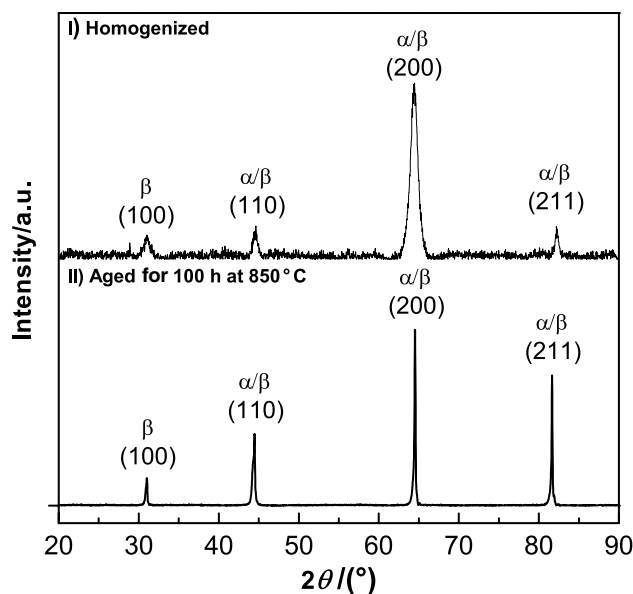
Even though the analysis of the microstructural characteristics of FAN2015 and FAN2823 alloys suggests the occurrence of a spinodal reaction, other complementary techniques, like transmission electron microscopy, are necessary for the complete assessment of this phenomenon.

Table 2 shows a comparison between the compositions of α and β' phases in FAN2823 and FAN1510 alloys after 100 h of aging at 850 °C. It is evident that higher Ni and Al contents in the alloy promote an increase in the concentration of these elements in the individual phases.

4 Structural characterization

Figure 4 shows XRD spectra of FAN2015 alloy after: (I) homogenizing and quenching and (II) homogenizing, quenching and aging for 100 h at 850 °C. It can be observed that the alloy shows the characteristic (100) peak of β' phase in the as-quenched condition, which indicates the presence of this phase at 1100 °C in concordance with the phase equilibrium diagrams [18]. The broad peaks could be caused by the presence of diffuse sidebands due to composition fluctuations [33] that take place before the phase separation by spinodal decomposition.

XRD spectra after aging for 100 h at 850 °C also shows the presence of (100) peak. The refinement of the peaks indicates that the phase separation takes place and both phases are closer to their equilibrium composition. It must be noted that even if the intensity of the peaks changes from one condition to another, this does not indicate a change in phase fraction. The reason for this is that the casting process promotes the formation of large columnar grains that can be interpreted by XRD as a strong texture. Also, due to the similar structure and lattice parameters, the characteristic peaks of α phase overlap with most peaks of β' phase.

**Fig. 4** XRD patterns of FAN2015 alloy

5 Growth kinetics

Developed by Lifshitz and Slyozov [34] and independently by Wagner [35], the theory now known as the Lifshitz–Slyozov–Wagner (LSW) was initially proposed to describe the growth of spherical precipitates in liquid–solid systems where the precipitate volume fraction is close to zero. The theory was further extended for precipitation in solid–solid systems and has been used as reference in systems with considerably larger volume fractions.

As stated in Sect. 3, in the FAN1210 and FAN1510 alloys, the aging process promotes a change in the precipitate morphology which deviates from the initial spherical shape. In the case of FAN2015 alloy, the initial morphology is irregular. Having this in mind, the equivalent radius of a sphere with equal volume must be used as parameter in order to analyze the size evolution. FAN2823 alloy was not considered for this analysis since β' phase is fully interconnected.

Figure 5a presents the evolution of the equivalent mean radius with aging. The trend is an increase in the mean radius with Ni and Al contents. The standard deviation is considerably higher in FAN2015 alloy, where small cuboidal-shaped precipitates coexist with considerably larger plate-shaped and irregular precipitates as presented in Sect. 3. Figure 5b shows the $\ln \bar{r} - \ln t$ plots of FAN1210, FAN1510 and FAN2015 alloys, where \bar{r} is the mean radius at time t . The standard deviation is below 5%. Besides the evident effect of larger precipitate size related to higher NiAl fraction, all plots present similar slopes, which are

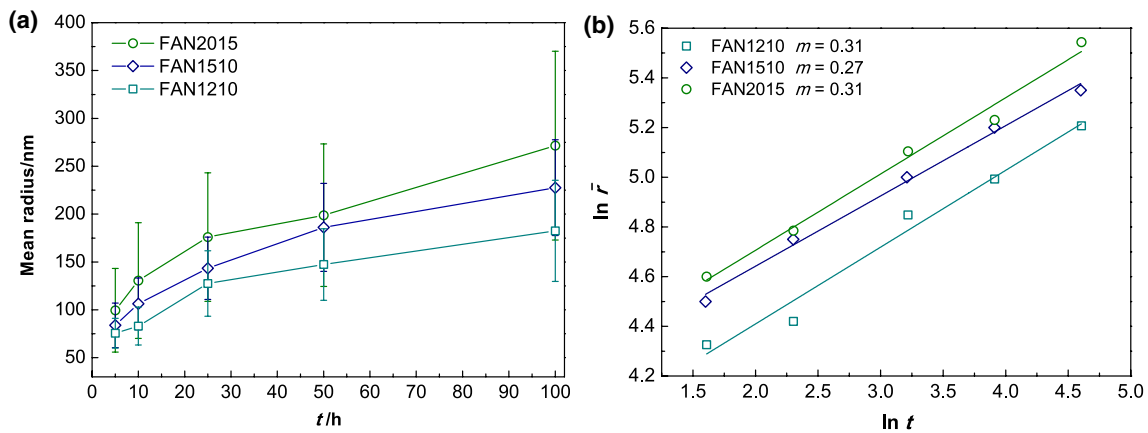


Fig. 5 Change of mean radius during aging (a) and $\ln \bar{r} - \ln t$ plot (b)

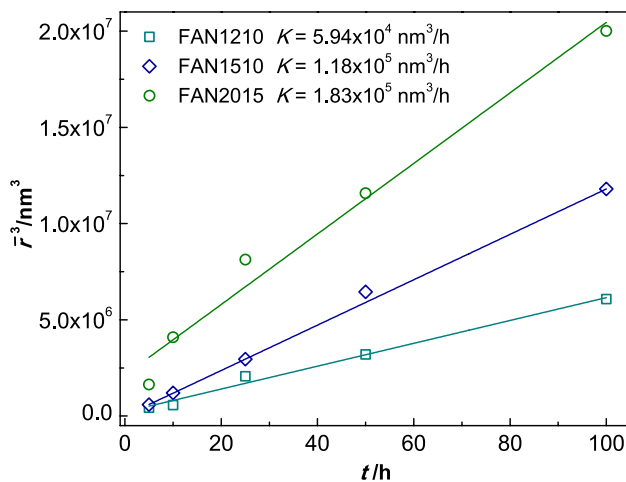


Fig. 6 Evolution of cube of mean radius during aging at 850 °C

close to $m = 1/3$ estimation of LSW theory. This means that the coarsening process is controlled by diffusion.

LSW theory states that the volumetric change in the precipitates is given by the following equation:

$$\bar{r}^3(t) - \bar{r}^3(0) = Kt \quad (1)$$

where K is the kinetic constant, which is dependent on temperature.

Figure 6 shows \bar{r}^3 vs. time plot of the studied alloys. It can be observed that the three alloys present a linear behavior. From this plot, the kinetic constant of the coarsening process can be obtained. In this case, the highest kinetic constant was found in FAN2015 alloy which is also the composition with higher β' fraction. Overall, the kinetic constant increases with higher Ni and Al content. The kinetic constants and β' area fraction of the three alloys are presented in Table 3 for comparison.

Table 3 Parameters of analyzed alloys

Alloy	m	$K/(\text{nm}^3 \text{ h}^{-1})$	f_A
FAN1210	0.31	5.94×10^4	0.13
FAN1510	0.27	1.18×10^5	0.19
FAN2015	0.31	1.81×10^5	0.44

Several aspects could affect the coarsening kinetics. An extension of LSW theory was developed for binary systems with nonzero solubility and non-ideal solution thermodynamics [36]. In this model, the corresponding rate constant for the time evolution of the average particle radius is given by

$$K = \frac{(8DV_\beta\sigma_{\alpha\beta})}{9(c_\beta^e - c_\alpha^e)^2 G''_\alpha} \quad (2)$$

where c_α^e and c_β^e are the equilibrium compositions of α and β phases, respectively; V_β is the molar volume of β phase; G''_α is the second derivative of the molar Helmholtz energy of α phase; D is the diffusion coefficient; and $\sigma_{\alpha\beta}$ is the specific interfacial energy. The overall larger precipitate size in alloys with higher Ni and Al contents implies an increase in the interfacial energy, and in the case of FAN2015 alloy, a partial loss of coherency as observed in the irregular shape of the β' phase after extended aging. The diffusion coefficient is strongly affected by composition [37]. Studies by molecular dynamics [38] indicate that higher Ni content promotes an increase in the vacancy diffusion of BCC phase in Fe–Ni system. All of these factors promote higher coarsening kinetics as observed.

Figure 7 shows the size distributions of the analyzed alloys after aging at 850 °C for 10 and 100 h. The theoretical distribution of LSW theory is also plotted for comparison.

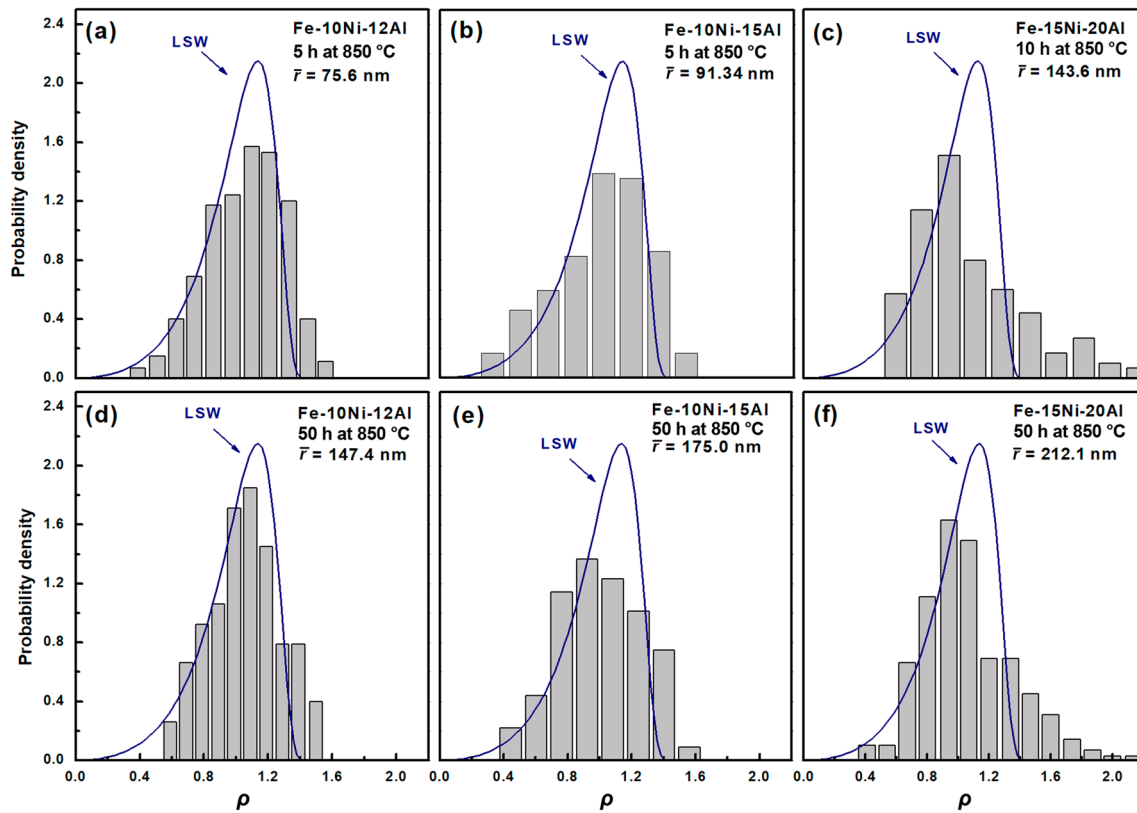


Fig. 7 Evolution of size distributions during aging

The probability density from experimental measurements was calculated using the following equation [28]:

$$\rho^2 f(\rho) = (N_{(r,r+\Delta r)} / \sum N_{(r,r+\Delta r)}) \left(\frac{\bar{r}}{\Delta r} \right) \quad (3)$$

where $N_{(r,r+\Delta r)}$ is the number of particles in the given interval; and Δr is the class size. x -axis corresponds to the normalized radius, ρ , which is defined as r/\bar{r} .

It can be observed that FAN1210 alloy which has the lowest Ni and Al contents, and therefore a smaller volumetric fraction of β' phase, is the closest to the theoretical LSW curve. On the other hand, in the alloys with a larger β' phase fraction, the size distributions become broader and present a higher deviation from the theoretical curve. This behavior has been studied in elastically stressed systems [39] and is attributed to an increase in the effects of elastic energy caused by a larger average particle size.

6 Mechanical characterization

The average hardness of all alloys after 10 and 100 h of aging at 850 °C is shown in Fig. 8. The standard deviation is below 6%. It can be observed that hardness tends

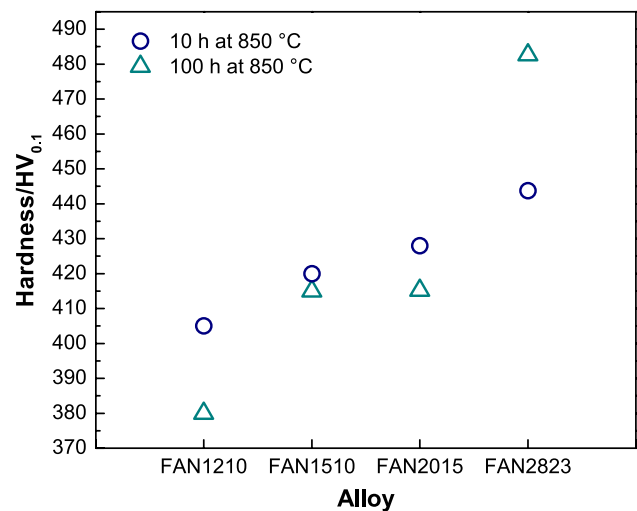


Fig. 8 Hardness of alloys after 10 and 100 h of aging

to increase with higher Ni and Al contents, and therefore with higher β' volumetric fraction. This statement also stays true after 100 h of aging, even though the hardness of the FAN1210, FAN1510 and FAN2015 alloys decreased due to the coarsening of β' particles.

The only exception is FAN2823 alloy, where hardness presented a noticeable increment. Very similar behavior was observed in Fe–Mn–Ni–Al alloys that undergo spinodal decomposition and present a modulated microstructure [20]. This behavior has been attributed to the amplitude increase in composition waves and the associated strain field. Regarding the mechanical properties of modulated microstructures, Cahn [40] predicted that the yield stress should be proportional to $A^2\lambda$, where A is the amplitude of the composition modulation and λ is the wavelength. However, the calculations provided by the model of Cahn are reported to be below experimental values. Another approach to this problem is proposed by Kato et al. [41], who explained the phenomenon in terms of the internal coherency stress fields caused by the composition modulation. They propose that the yield stress should be proportional to A and independent of λ . A reasonable agreement with experimental data has been reported [42]. In order to relate the behavior of FAN2823 alloy to any of these models in subsequent studies, a very precise determination of the wavelength and the amplitude of the composition modulation along with macroscopic mechanical testing will be required.

7 Conclusions

1. Increasing Ni and Al contents promotes a higher β' phase fraction in concordance with the phase equilibrium diagrams. The alloys with combined Ni and Al contents higher than 35% showed signs of spinodal decomposition, while alloys with lower Ni and Al contents followed classical nucleation.
2. The coarsening process in FAN1210, FAN1510 and FAN2015 alloys is controlled by diffusion as predicted by LSW theory. Increasing Ni and Al contents promoted higher values of the coarsening kinetic constant.
3. From the analyzed alloys, FAN1210 composition presented the lowest coarsening kinetics, which would be beneficial to withstand high-temperature conditions.
4. The hardness of the alloys was dependent of the volumetric fraction of β' phase. A higher fraction of the intermetallic promotes an increase in hardness. Nevertheless, this has been correlated with a very low room-temperature ductility.

Acknowledgements The authors would like to thank Consejo Nacional de Ciencia y Tecnología (CONACYT) (Project CB-2013 No. 222459) and IPN-SIP-BEIFI for their financial support. Special thanks are due to G. Gonzalez, A. Diaz, R. Piña, J. Bernal and E. Arriaga for their technical assistance.

References

- [1] R. Viswanathan, J.F. Henry, J. Tanzosh, G. Stanko, J. Shingledecker, B. Vitalis, R. Purgert, *J. Mater. Eng. Perform.* 22 (2013) 2904–2915.
- [2] Z. Sun, C.H. Liebscher, S. Huang, Z. Teng, G. Song, G. Wang, M. Asta, M. Rawlings, M.E. Fine, P.K. Liaw, *Scripta Mater.* 68 (2013) 384–388.
- [3] R.D. Noebe, R.R. Bowman, M.V. Nathal, *Int. Mater. Rev.* 38 (1993) 193–232.
- [4] K. Bochenek, M. Basista, *Prog. Aerospace Sci.* 79 (2015) 136–146.
- [5] P.R. Munroe, M. George, I. Baker, F.E. Kennedy, *Mater. Sci. Eng. A* 325 (2002) 1–8.
- [6] M.A. Muñoz-Morris, D.G. Morris, *Mater. Sci. Eng. A* 444 (2007) 236–241.
- [7] C. Stallybrass, G. Sauthoff, *Mater. Sci. Eng. A* 387–389 (2004) 985–990.
- [8] C. Stallybrass, A. Schneider, G. Sauthoff, *Intermetallics* 13 (2005) 1263–1268.
- [9] N.Q. Vo, C.H. Liebscher, M.J.S. Rawlings, M. Asta, D.C. Dunand, *Acta Mater.* 71 (2014) 89–99.
- [10] M. Doi, T. Miyazaki, T. Wakatsuki, *Mater. Sci. Eng.* 67 (1984) 247–253.
- [11] D.A. Porter, K.E. Easterling, M.Y. Sherif, *Phase transformations in metals and alloys*, 3rd ed., CRC Press, Boca Raton, USA, 2008.
- [12] M.J.S. Rawlings, C.H. Liebscher, M. Asta, D.C. Dunand, *Acta Mater.* 128 (2017) 103–112.
- [13] C.H. Liebscher, V.R. Radmilović, U. Dahmen, N.Q. Vo, D.C. Dunand, M. Asta, G. Ghosh, *Acta Mater.* 92 (2015) 220–232.
- [14] G. Song, S.J. Hong, J.K. Lee, S.H. Song, S.H. Hong, K.B. Kim, P.K. Liaw, *Scripta Mater.* 161 (2019) 18–22.
- [15] L. Sun, T.H. Simm, T.L. Martin, S. McAdam, D.R. Galvin, K.M. Perkins, P.A.J. Bagot, M.P. Moody, S.W. Ooi, P. Hill, M.J. Rawson, H.K.D.H. Bhadeshia, *Acta Mater.* 149 (2018) 285–301.
- [16] S. II Baik, M.J.S. Rawlings, D.C. Dunand, *Acta Mater.* 144 (2018) 707–715.
- [17] C. Ferreira-Palma, E. Contreras-Piedras, N. Cayetano-Castro, M.L. Saucedo-Muñoz, V.M. Lopez-Hirata, J.L. González-Velázquez, H.J. Dorantes-Rosales, *Metall. Mater. Trans. A* 48 (2017) 5285–5293.
- [18] S.M. Hao, T. Takayama, K. Ishida, T. Nishizawa, *Metall. Trans. A* 15 (1984) 1819–1828.
- [19] K. Binder, P. Fratzl, in: G. Kostorz (eds.), *Phase Transformations in Materials*, Wiley-VCH Verlag GmbH & Co. KGaA, Weinheim, Germany, 2005, pp. 409–480.
- [20] J.A. Hanna, I. Baker, M.W. Wittmann, P.R. Munroe, *J. Mater. Res.* 20 (2005) 791–795.
- [21] M. Schober, R. Schnitzer, H. Leitner, *Ultramicroscopy* 109 (2009) 553–562.
- [22] H. Leitner, M. Schober, R. Schnitzer, S. Zinner, *Mater. Sci. Eng. A* 528 (2011) 5264–5270.
- [23] R. Rahimi, P. Pekker, H. Biermann, O. Volkova, B.C. De Cooman, J. Mola, *Mater. Des.* 111 (2016) 640–645.
- [24] T. Chen, C.M. Parish, Y. Yang, L. Tan, *Mater. Sci. Eng. A* 720 (2018) 110–116.
- [25] Y.S. Huang, X.G. Wang, C.Y. Cui, J.G. Li, L.H. Ye, G.C. Hou, Y.H. Yang, J.L. Liu, J.D. Liu, Y.Z. Zhou, X.F. Sun, *Mater. Sci. Eng. A* 773 (2020) 138886.
- [26] A.J. Bradley, *J. Iron Steel Inst.* 163 (1949) 19–30.
- [27] N. Cayetano-Castro, H.J. Dorantes-Rosales, V.M. López-Hirata, J.J. Cruz-Rivera, J. Moreno-Palmerin, J.L. González-Velázquez, *Rev. Metal.* 44 (2008) 162–169.
- [28] A.J. Ardell, R.B. Nicholson, *J. Phys. Chem. Solids* 27 (1966) 1793–1794.

- [29] P. Fratzl, O. Paris, *Phase Transitions* 67 (1999) 707–724.
- [30] Y.H. Sohn, A. Puccio, M.A. Dayananda, *Metall. Mater. Trans. A* 36 (2005) 2361–2370.
- [31] M. Fährmann, P. Fratzl, O. Paris, E. Fährmann, W.C. Johnson, *Acta Metall. Mater.* 43 (1995) 1007–1022.
- [32] E.O. Avila-Dávila, S. Lezama-Álvarez, M.L. Saucedo-Muñoz, V.M. López-Hirata, J.L. González-Velázquez, M. Pérez-Labra, *Rev. Metal.* 48 (2012) 223–236.
- [33] Z. He, M.C. Chaturvedi, *Mater. Sci. Technol.* 9 (1993) 642–646.
- [34] I.M. Lifshitz, V.V. Slyozov, *J. Phys. Chem. Solids* 19 (1961) 35–50.
- [35] C. Wagner, *Z. Elektrochemie* 65 (1961) 581–594.
- [36] R. Wagner, R. Kampmann, P.W. Voorhees, in: G. Kostorz (eds.), *Phase Transformations in Materials*, Wiley-VCH Verlag GmbH & Co. KGaA, Weinheim, Germany, 2005, pp. 309–408.
- [37] K. Hirano, M. Cohen, B.L. Averbach, *Acta Metall.* 9 (1961) 440–445.
- [38] N. Anento, A. Serra, Y. Osetsky, *Acta Mater.* 132 (2017) 367–373.
- [39] K. Thornton, N. Akaiwa, P.W. Voorhees, *Acta Mater.* 52 (2004) 1365–1378.
- [40] J.W. Cahn, *Acta Metall.* 11 (1963) 1275–1282.
- [41] M. Kato, T. Mori, L.H. Schwartz, *Acta Metall.* 28 (1980) 285–290.
- [42] K. Sato, K. Tagawa, Y. Inoue, *Mater. Sci. Eng. A* 111 (1989) 45–50.